

RECEIVER FUNCTION ANALYSIS OF THE MANTLE TRANSITION ZONE BENEATH CAPE VERDE

Amy Y. Amatya

A SENIOR THESIS
PRESENTED TO THE FACULTY
OF GEOSCIENCES PRINCETON UNIVERSITY
IN CANDIDACY FOR THE DEGREE
OF BACHELOR OF ARTS

RECOMMENDED FOR ACCEPTANCE
BY THE DEPARTMENT OF
GEOSCIENCES
Adviser: Frederik J. Simons

April 24, 2021

Abstract

The Cape Verde Islands are a hotspot believed to be fed by a mantle plume that is stationary relative to the overlying plate. Characterization of the mantle transition zone underlying Cape Verde offers an opportunity for improving our understanding of hotspot formation and mantle dynamics. However, the region is seismically understudied and undersampled, hence models have remained underconstrained. Seismic data recorded on noisy island stations are highly variable in quality. This study aims to shed light on the structure and formation of Cape Verde's hotspot through a receiver function analysis of the mantle transition zone in the region. To this end, I test the applicability of a signal-filtering and receiver function-generating toolkit developed by Burky et al. (2021). My analysis yields evidence of depressed 410 km and 660 km discontinuities, in line with the work of Helffrich et al. (2010). This challenges previous findings of a thin transition zone beneath Cape Verde, calling for an alternate explanation of the thermal source of the island's hotspot.

Contents

Abstract	iii
Acknowledgements	iv
List of Figures	vi
Main Text	1
Introduction	1
Mantle Transition Zone (MTZ)	2
Seismic Methods	4
Data: Limitations, Considerations	5
Methods	8
Data Processing	8
Receiver Functions and Stacking	14
Results	15
Discussion	21
Conclusions	22
Appendix	23
References	24

List of Figures

1	Cape Verde seismic context map	1
2	IASP91 velocity profile	3
3	Event depth and magnitude distribution map	6
4	Magnitude frequency distribution	7
5	Seismograms of different size-depth configurations	8
6	Wave arrival and particle motion for small, shallow event	10
7	Wave arrival and particle motion for large, deep event	11
8	Wave arrival and particle motion for large, shallow event	12
9	Seismogram processing	13
10	SACV v. SVMA Receiver Function for 2014 Iquique Quake	14
11	Reference receiver function	15
12	Gaussian width stacking	16
13	Corner frequency stacking	16
14	Epicentral distance stacking contour plot	17
15	SACV Location 00 Stack	18
16	SACV Location 10 Stack	19
17	Magnitude and depths of stacked RFs	19
18	SVMA Stack	20

Introduction

Mantle hotspots are responsible for volcanism and island formation, yet their origin is controversial (Davies, 1999). Morgan (1971) suggested that plumes of warm material rising from the lower mantle feed hotspots, Allègre (2002) supported an origin in the mantle transition zone (MTZ) extending from 410 km to 660 km, and Anderson (2000) argued that they can be explained by the production of hot material by shallow stresses on lithospheric plates. The diameters, temperatures, and depths of hotspot origins are poorly constrained because they rely either on models created from the indirect observations of surface bathymetry, gravity, and heat flow (Zhao, 2001), or through inferences made using depth-limited and often noisy seismic data from island stations (Helffrich et al., 2010).

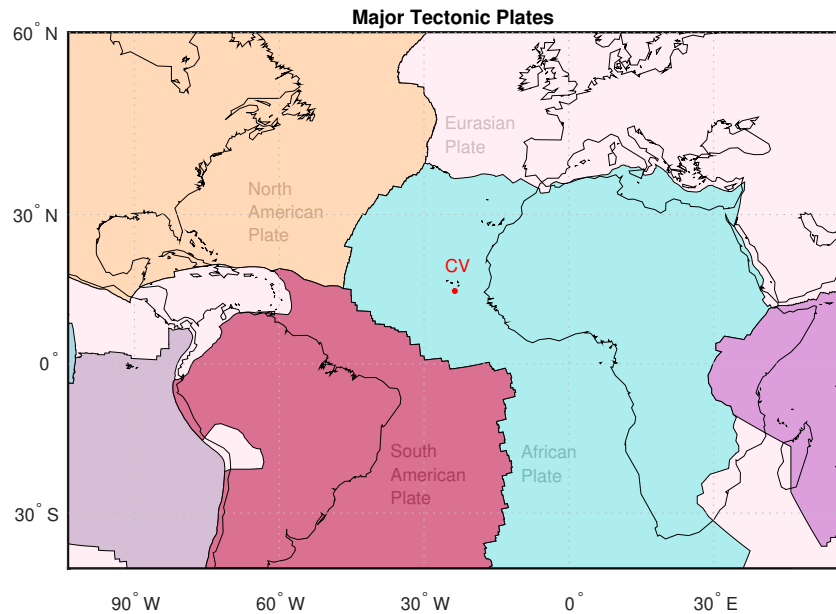


Figure 1: Cape Verde relative to major tectonic plates. Cape Verde sits on the slow-moving African Plate, whose western edge is a divergent boundary (Burke & Wilson, 1972).

Thus, the provenance of the Cape Verde hotspot remains murky. Cape Verde is comprised of ten volcanic islands off the westernmost point of Africa. The archipelago is located on the slow-moving African Plate (Fig. 1) where its hotspot is nearly stationary relative to the overlying

lithospheric plate Holm et al. (2008) in contrast with the better-studied hotspots of, for example, Yellowstone and the Hawaiian Islands, whose overlying plates move within the hotspot reference frame (Helffrich et al., 2010). This means that Cape Verde is uniquely positioned to offer a view of plume and heat flow dynamics largely unobstructed by lithospheric movement (Liu & Zhao, 2014). The motivation behind this study of seismic waves beneath Cape Verde is, then, twofold: to shed light on the mantle processes responsible for Cape Verde's formation and volcanism in particular, and to employ the hotspot's unique fixity to gain a better understanding of hotspot origins in general.

Mantle Transition Zone (MTZ)

The mantle transition zone (MTZ) is central to our seismological investigation of the Cape Verde hotspot. Its upper and lower boundaries are defined by seismic wave velocity discontinuities occurring at around 410 km and 660 km depth, respectively (Davies, 1999). Wave velocity is primarily a function of the elastic moduli and density of the medium through which a wave passes, which in a seismic context means the chemical, compositional and thermal properties of Earth's interior. These discontinuities in the MTZ, hereafter referred to as 'the 410' and 'the 660,' coincide with increases in wave speeds associated with the pressure-induced phase transformation of olivine to wadsleyite at the 410, and ringwoodite to perovskite and magnesiowüstite at the 660 (Ito & Takahashi, 1989). What results are positive velocity jumps at the 410 and 660 as illustrated in Fig. 2, causing waves to either reflect or convert between *P*- and *S*-types upon reaching those boundaries. The Clapeyron slopes of these phase transformations indicate that an increase in temperature, such as that caused by mantle plume activity, is expected to deepen the 410 and shoal the 660, leading to a thinner transition zone thickness (TZT) (Bina & Helffrich, 1994). The opposite is true of a temperature decrease seen in, for example, subduction zones (Flanagan & Shearer, 1998). In other words, the thickness of the mantle transition zone—as determined by the behavior of *P*- and *S*-waves encountering the 410 and 660—becomes a proxy for the thermal structure of the upper mantle (Andrews & Deuss, 2008).

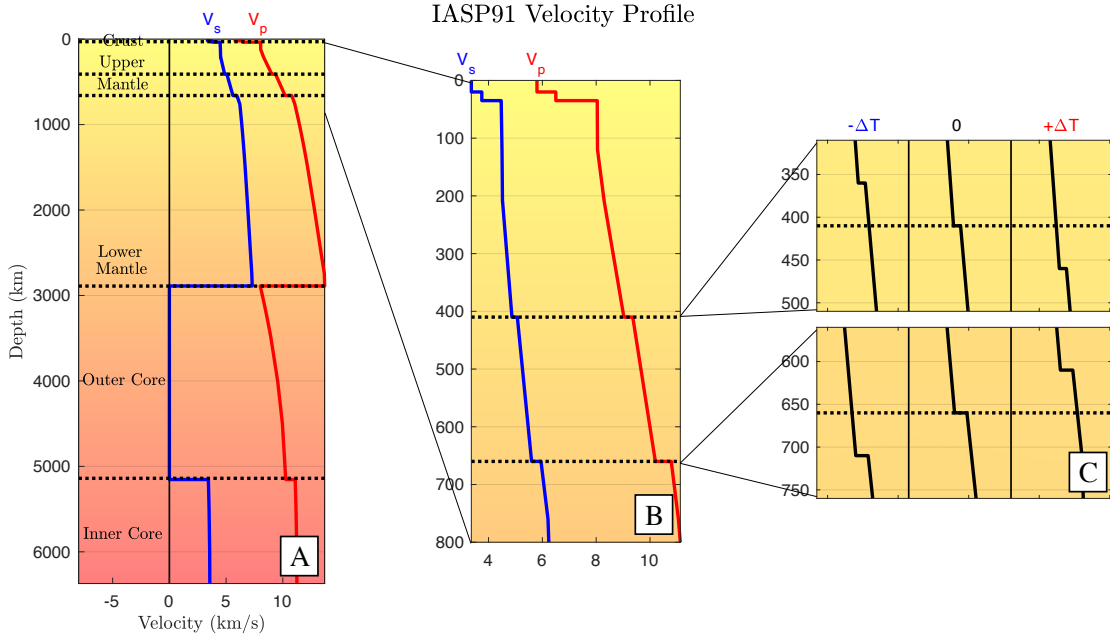


Figure 2: P - and S -wave velocities in the IASP91 model of Earth’s interior. (a) Velocity profile of whole interior (b) Positive V_p and V_s jumps at around 410 km and 660 km depth in the upper mantle. (c) The depth of discontinuity varies directly with an increase in temperature at the 410 and inversely at the 660. The specific behavior of these velocity responses in the MTZ underlying Cape Verde remains inconclusive.

The characterization of the mantle transition zone beneath Cape Verde is disputed. Vinnik et al. (2012) and Saki et al. (2015) found that the TZT is reduced, suggesting that Earth’s mantle feeds the hotspot from within or below the MTZ. On the contrary, Helffrich & Wood (2001) found a normal TZT, arguing that this either means the hotspot source lies at a depth above the lower mantle, or that the hotspot origin is not accompanied by significant thermal change. Montelli et al. (2006) suggest that Cape Verde overlies a plume that merges with the Azores and Canary plumes at the base of the mantle, but assessments of the TZT in this broader North Atlantic region have yielded equally inconclusive results. While Silveira et al. (2010) finds a normal TZT below the Azores platform, both Lawrence & Shearer (2006) and Gu & Dziewonski (2002) observe a thinned TZT.

Seismic Methods

The seismic methods used in these studies fall under two categories: SS precursors, and receiver functions. The SS precursor method makes use of *S*-waves that reflect off discontinuities and arrive before the main SS wave. Their long-period nature gives them the advantage of better capturing weak discontinuity signals of the 660 compared to PS receiver functions. However, they exhibit a relatively low signal-to-noise ratio, have a large Fresnel zone that can preclude resolving small features such as mantle plumes, and depend on an available and even distribution of global seismic stations (Deuss, 2007; Shearer et al., 1999). Instead, receiver functions use data with higher signal-to-noise ratios and smaller spatial resolutions, though they only examine individual seismic stations in isolation (Houser et al., 2008). Saki et al. (2015) propose that diverging TZT results may in part arise from these two different methodologies, based on the observation that Silveira et al. (2010) discovered a normal TZT using the receiver function method and Lawrence & Shearer (2006) discovered a thinned TZT based on SS precursors. Still, Deuss (2007)'s finding of a normal TZT beneath Cape Verde using SS precursors and Vinnik et al. (2012)'s finding of a thin TZT using receiver functions demonstrates the lack of consensus not only on specific properties of the mantle transition zone beneath Cape Verde, but also on the preferred method for approaching this investigation in the first place.

This study will look at the behavior of *P*- and *S*-waves in the MTZ through receiver-function analysis to provide another perspective on this debate. Receiver functions make use of the fact that waves approaching a seismic station undergo a series of phase conversions between *P* and *S* upon encountering a discontinuity (Shearer, 2009). We are specifically interested in *P*- to *S*-converted phases (*Ps*). The difference in arrival time between waves converted at the 410 (*P410s*) and the 660 (*P660s*) carries information about the depth of phase conversion, and thus the thickness of the transition zone. Receiver functions utilize data from single receiver sites, originally in the form of three-component seismograms, which acts to isolate the effects of different sources and ray paths (Kind et al., 2012).

Data: Limitations, Considerations

Discrepant results in characterization of the MTZ underlying Cape Verde reflect limitations in seismic data which are tied to (1) the nature of earthquakes within Earth, and (2) our ability to record such earthquakes. The quality and resolution of seismic data are bounded by the location, magnitude, and frequency of seismic events. The curvature of ray paths travelling away from an event source mean that, with a source too close to the receiver station—a distance that we define as 30° —the ray is unlikely to refract back toward Earth close enough to be intercepted by the station. Rays originating at an epicentral distance too great— 90° and beyond—are interfering with the outer core. This spatial range is represented by the lightened region in Fig. 3.

The upper limit of usable data is set by the increasing rarity of large events, and the increasing difficulty of capturing deep quakes (Fig. 3). The lower limit is a function of the sensitivity and reliability of seismometers and noise sources within Earth. Magnitude scales logarithmically, which poses a problem for retrieving the clean seismic signals associated with larger-magnitude events (Fig. 4).

With Cape Verde, the challenge of identifying clear *P*- and *S*-wave arrivals is amplified by the inherent noisiness of island seismic stations. In response, Burky et al. (2021) developed an automated method for receiver function quality control, featuring one filter on input component data and two filters on the resultant receiver functions in the context of Bermuda. This study will build on existing receiver function analyses of the MTZ beneath Cape Verde by applying this toolkit to seismic data from Cape Verde stations. The hope is that by incorporating 21 years of data from the Global Seismographic Network (GSN), along with this new filtration method, this study makes clearer our understanding of Cape Verde's origins and the formation of hotspots.

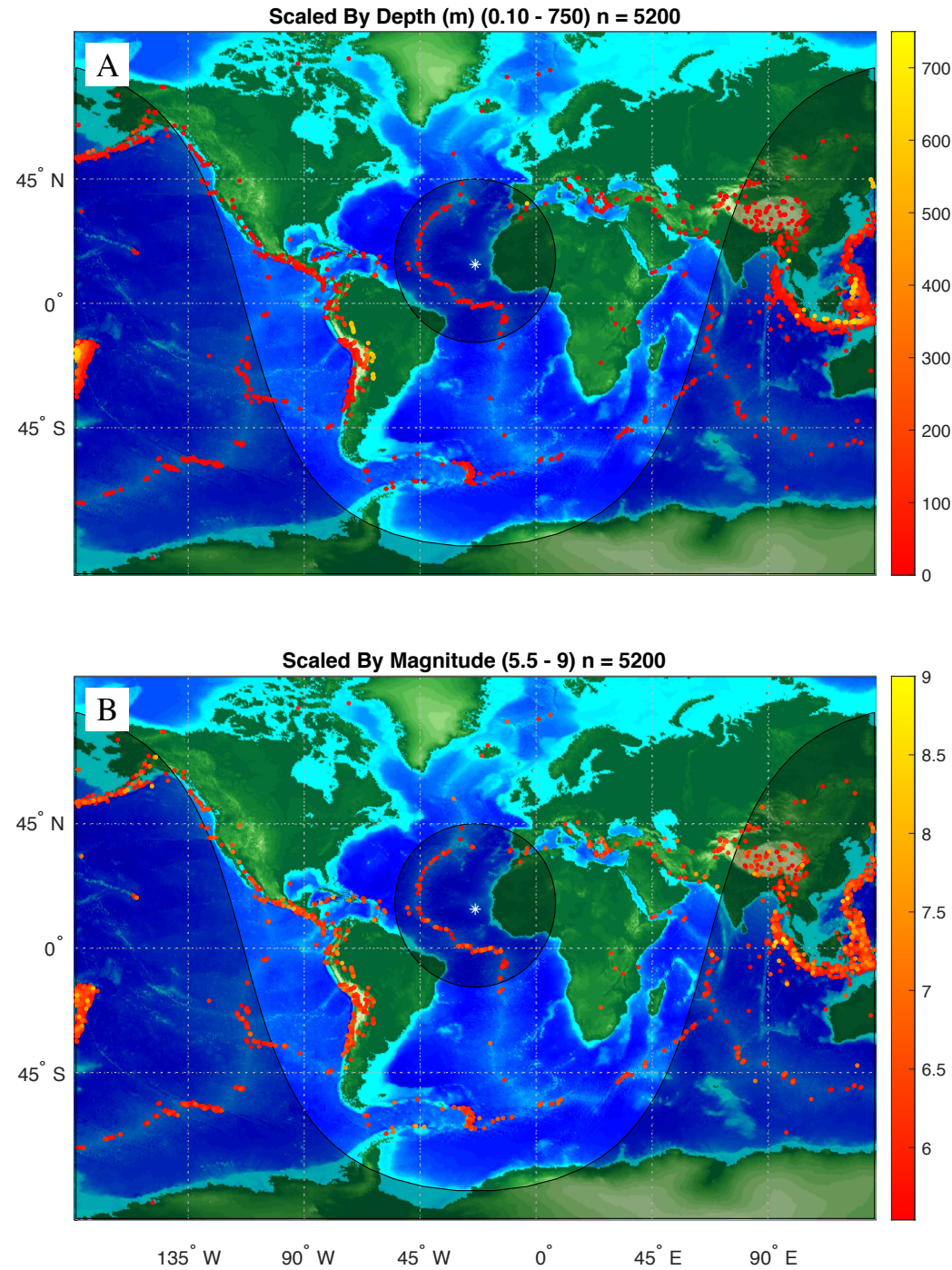


Figure 3: Geographic distribution of (a) event depth and (b) event magnitude. The light region represents Cape Verde's range of detection. Within this region, only events for which all three components exist are plotted, to accurately depict the data available for our study. Outside of this region, all available events are included to show the nature of depth and magnitude frequency.

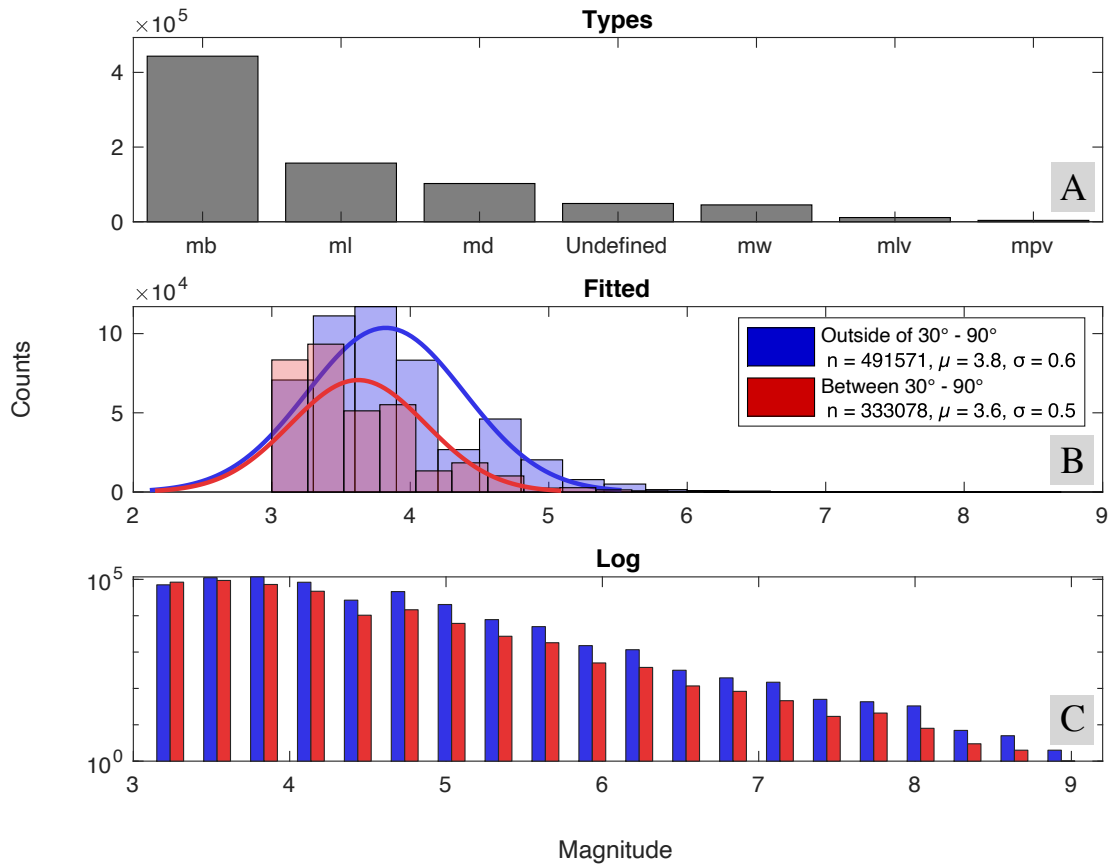


Figure 4: Frequency of event magnitudes in and outside of our available geographic range. Any events with depths greater than zero, representing non-earthquake interferences, were removed. (a) The five most common magnitude types are body-wave (mb/Mb), local (ml/MI), duration (md/MD), unspecified, and moment (Mw). (b) Events outside of Cape Verde's geographic range average a magnitude of 3.6 while those outside average 3.8. The greater number of events outside of this range contribute to both a larger standard deviation and higher number of large-magnitude quakes. (c) Log frequency of earthquake magnitudes.

Methods

Data come from Global Seismographic Network (GSN) station 'SACV' located on Santiago Island and AfricaArray station 'SVMA' on Sao Vicente via the Incorporated Research Institutions for Seismology Data Management Center (IRIS DMC). 'SACV' has been operational since 2000, while 'SVMA' only provides one year of data from 2014.

Data Processing

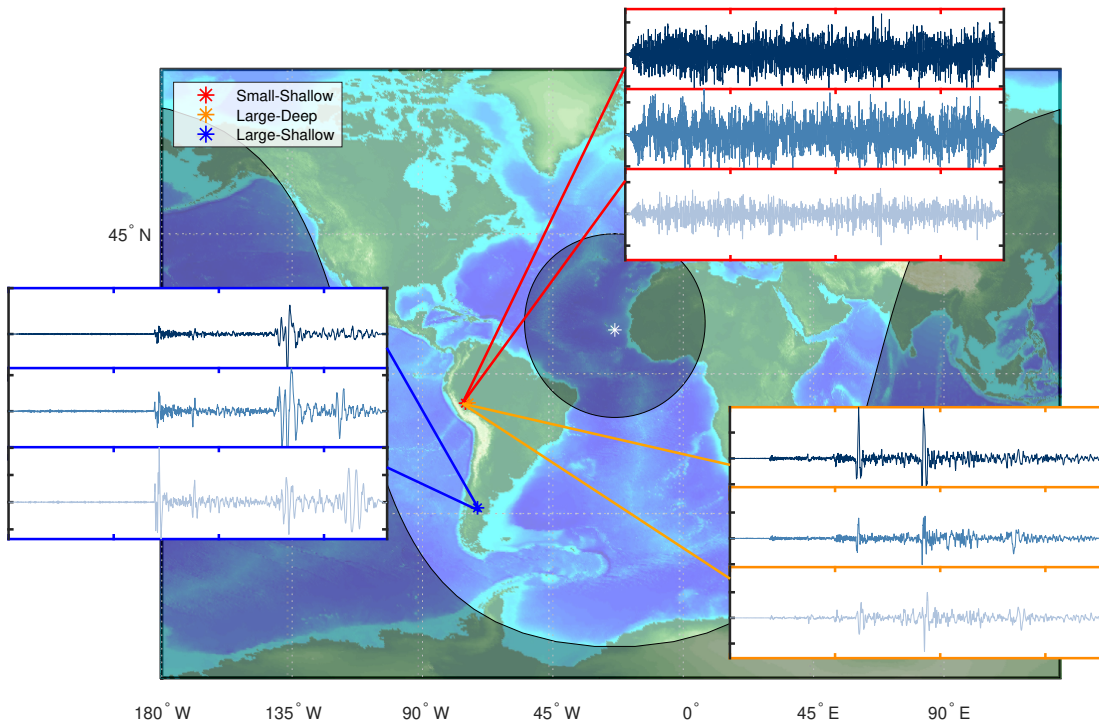


Figure 5: Rotated and instrument-corrected three-component seismograms. The small-shallow event, occurring on 10-30-2020, has magnitude 5.5 and depth 36 km. The large-deep event from 11-24-2015 has magnitude 7.6 and depth 620 km. The large-shallow event from 12-25-2016 has magnitude 7.6 and depth 38 km. The P - and S -wave arrivals, marked in Fig. 6, Fig. 8, and Fig. 7 are most discernible for the large shallow event, making the availability of such events desirable.

We select all events within an epicentral distance of 30° to 90° , that have a minimum magnitude of 6.0, and for which all three directional components exist. The effect of source depth and magnitude on signal clarity is depicted in Fig. 5. Shallow-sourced events have less interference.

ing noise to overcome in producing clear arrivals. However, large magnitudes allow even deep events to produce clear signals. The most pronounced arrivals with minimal pre-event noise are seen in the seismogram of a shallow, large-magnitude event (Fig. 5).

Particle motion is recorded on seismograms with respect to a North-South and East-West orientation. The next step after retrieval and frequency-dependent instrument response removal is to rotate the horizontal components into the source-station direction (radial) and its orthogonal (transverse) using the event azimuth. Wave arrival identification hinges on the specific, and distinct, behaviors of wave types in the three planes of motion. Rotation and the study of particle motion in these planes allow us to assess the quality and complexity of our dataset.

In the longitudinal *P*-wave, particle motion is parallel to the direction of propagation and thus expected to be linear in the radial-vertical plane, with a weak transverse signature. For torsional *S*-waves, particle motion is perpendicular to the direction of propagation and elliptical in the radial-transverse plane. With this in mind, waveforms of initial *P*- and *S*-arrivals for the three different size-depth traces remind us that seismic data are imperfect and variable. The highly noisy signal of the "small" (magnitude 5.5), shallow event lacks discernible arrivals and shows a weakly periodic relationship between radial and transverse movement for both the *P*- and *S*-wave (Fig. 6). This matters because previous receiver function analyses of the transition zone that use a minimum retrieval magnitude of 5.5, such as Gu & Dziewonski (2002), must rely on robust pre-processing filters in order to avoid diluting the more-meaningful signals associated with higher-magnitude, less frequent seismic events.

The initial *P*-wave signal of the large, deep event is also characterized by noisy and non-linear movement in the radial and transverse planes (Fig. 7). However, the *S*-wave has both a prominent arrival and narrow R-T movement, especially compared to the large-shallow event, whose depth presents fewer obstacles to wave propagation. The long period and weaker attenuation of *S*-waves makes them invaluable to the study of deeper-lying structures, such as the 660.

The large, shallow event, which characterizes an ideal trace within the bounds of retrievable data, demonstrates clear *P*- and *S*-arrivals in all three components. However, particle motion diagrams reveal limited radial movement and instead greater transverse movement (Fig. 6). Dispar-

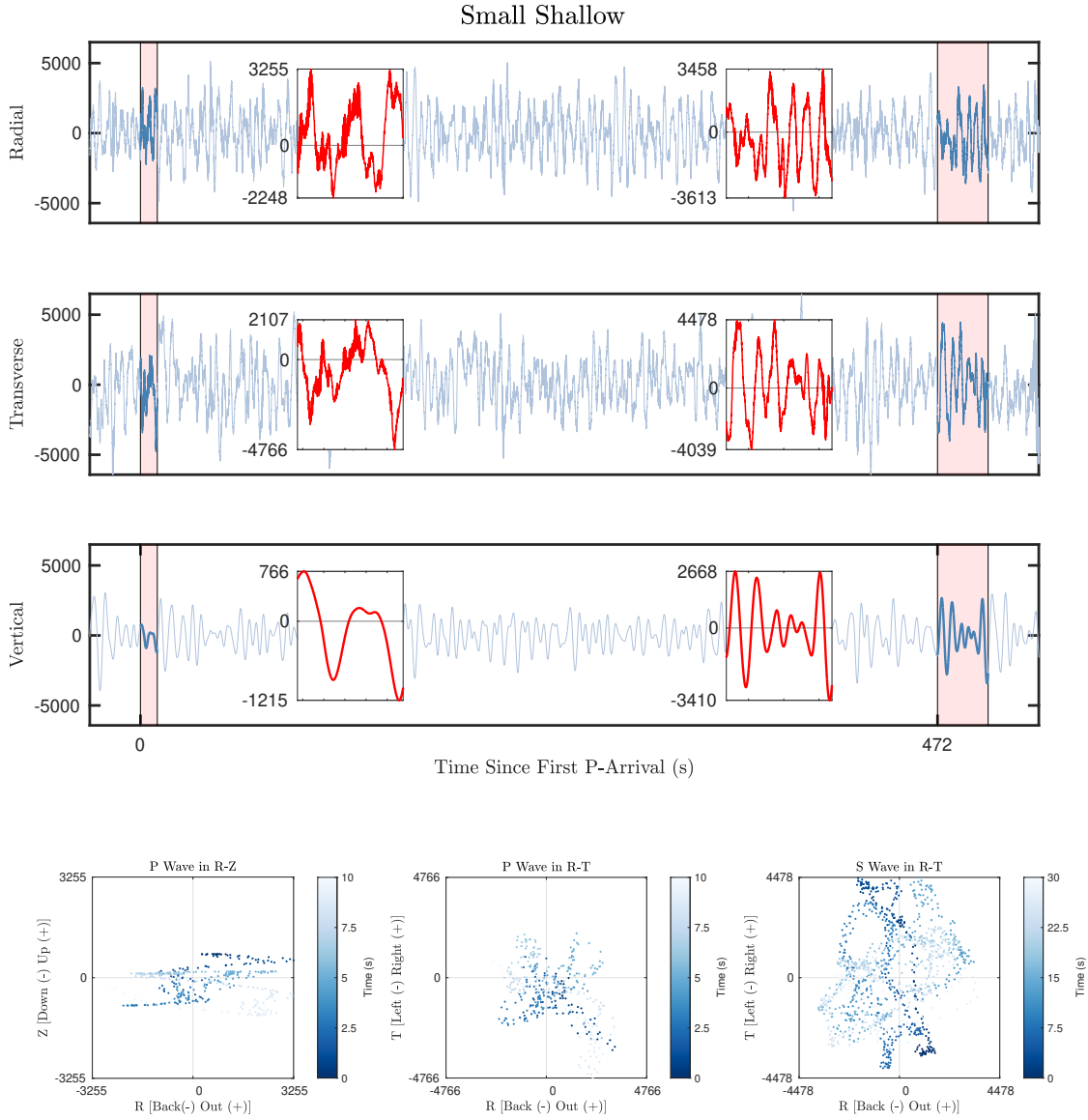


Figure 6: Radial, transverse, and vertical traces of a M_w 5.5, 36 km deep event. Superimposed red-marker plots emphasize the P -wave signature (left) and S -wave signature (right) of the underlying plot for the time window highlighted in red. This is 10 s after the P -arrival and 30 s after the S -arrival predicted by IASP91. Particle motion plots below depict the P wave in the radial-vertical plane, P wave in the radial-transverse plane, and S -wave in the radial-transverse plane. They are also limited to the highlighted time window, with the time progression of particle movement represented via color bar.

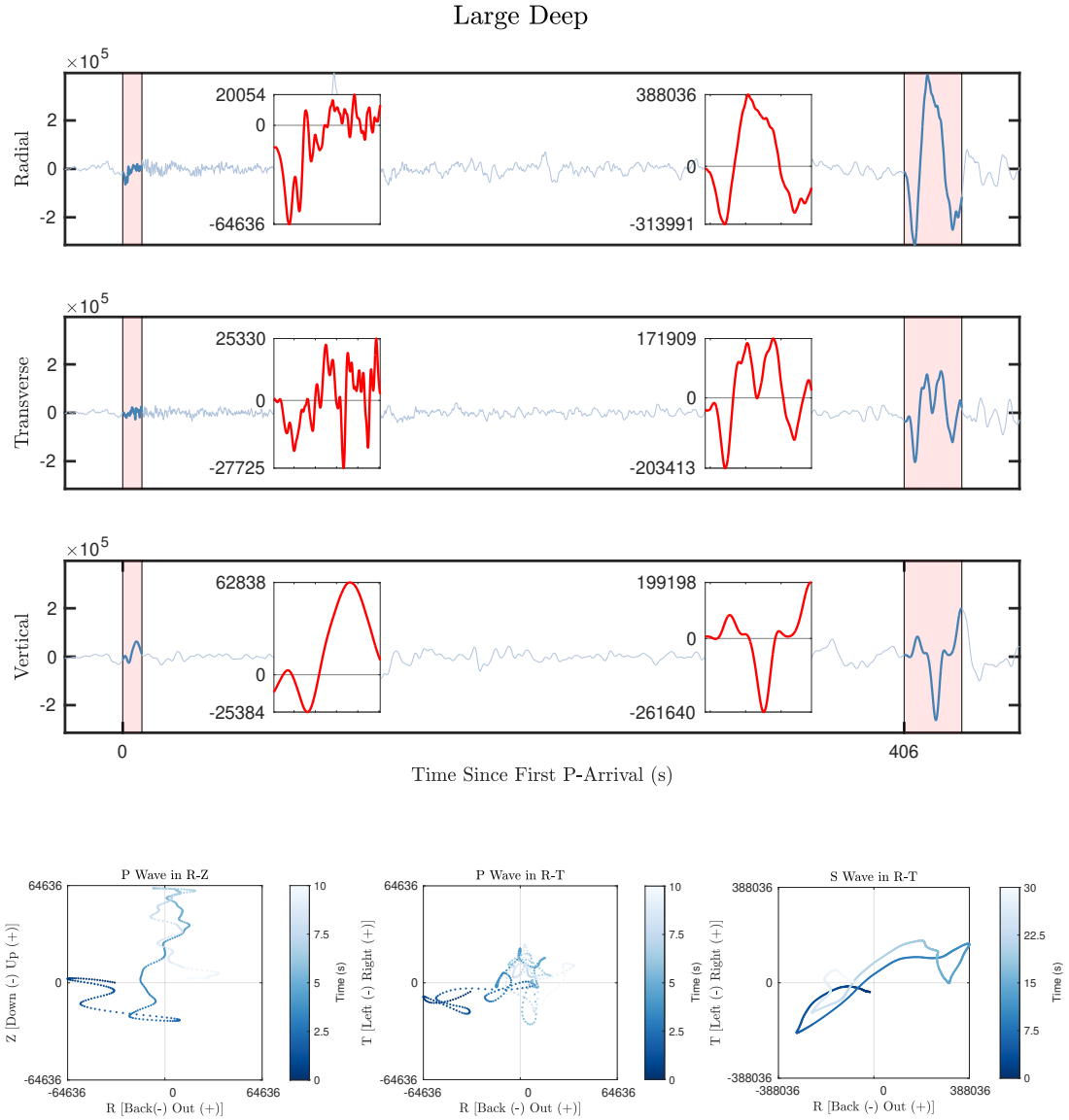


Figure 7: Seismograms, wave arrivals, and particle motions for a $M_w 7.6$, 620 km deep event.

ties between expected and observed seismic wave behavior signals at the complexity of Earth's interior, and this complexity backgrounds our use of seismic data in looking at the mantle.

After rotation, component data are filtered using a Butterworth bandpass filter from 50 Hz to 5 Hz based on the work of Crotwell & Owens (2005). Data are windowed from 30s before and

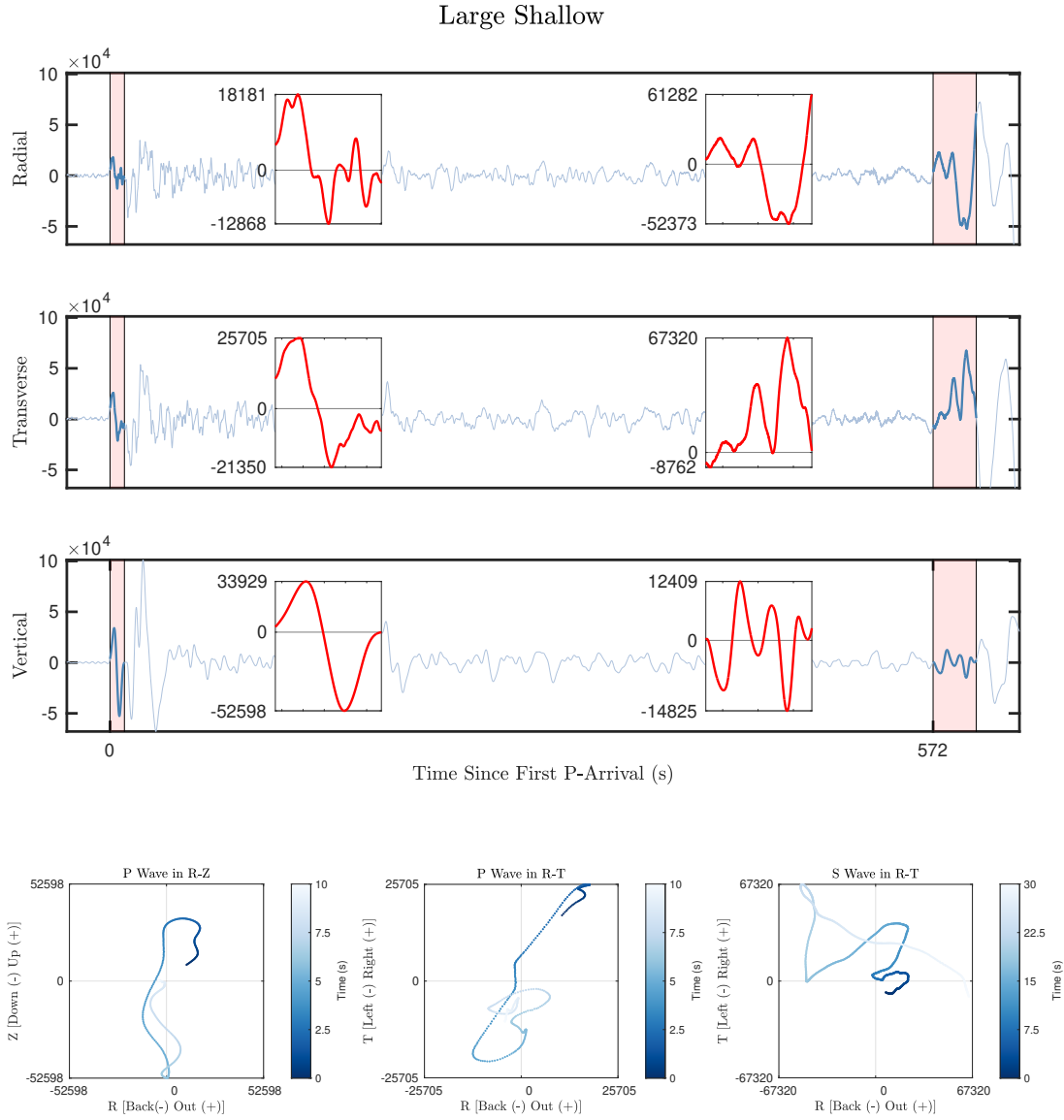


Figure 8: Seismograms, wave arrivals, and particle motions for a M_w 7.6, 38km deep event.

90s after the P -arrival time predicted by the IASP91 velocity model (Kennett & Engdahl, 1991).

The result of these transformations are shown in Fig. 9.

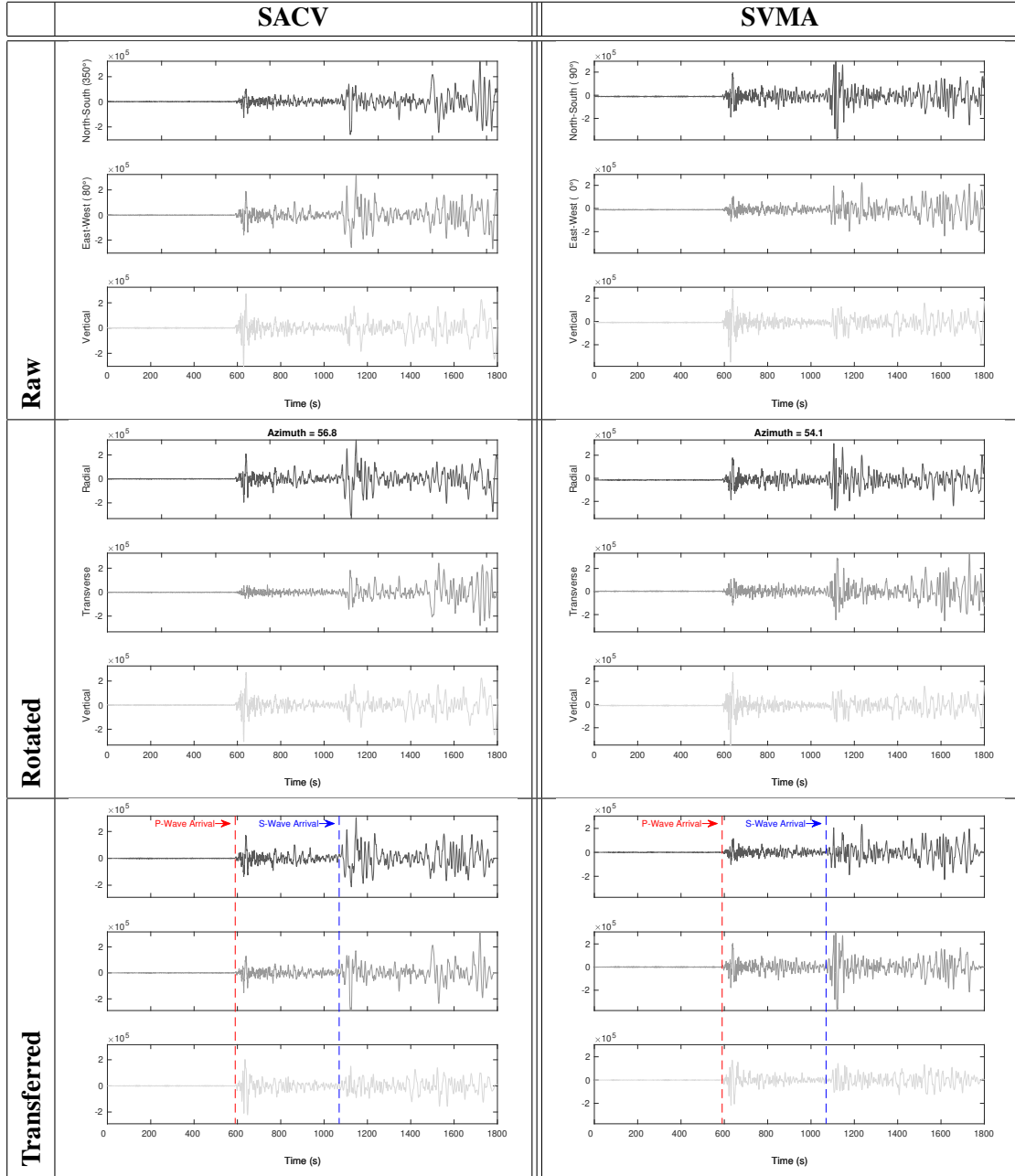


Figure 9: Data pre-processing: raw seismograms are rotated into event coordinate system and then instrument response is removed. Shown are three-component seismograms for stations SACV and SVMA. Both data record the same event—the 2014 Iquique earthquake—occurring on April 14, 2014. The source depth is 10 km with a magnitude of 8.1. Epicentral dist is 57.96km from SACV and 57.87 from SVMA.

Receiver Functions and Stacking

To calculate receiver functions, data undergo an iterative deconvolution method developed by Ligorria & Ammon (1999) which extracts the P -waveform from the vertical channel (where it appears most clearly), and repeatedly convolves the vertical component with the current receiver function representing the largest spike of a cross-correlation between vertical (U_Z) and radial (U_R) components (Ligorria & Ammon, 1999). This deconvolution only incorporates vertical component data with a signal-to-noise ratio greater than equal to 4.0, following the work of Gao & Liu (2014), and for which the fit between U_R and the currently convolved receiver function is greater than or equal to 0.8. A Gaussian width of 1.0 is used to isolate and fit the first pulses in the receiver function and U_R . Example outputs of this process are shown in Fig. 10. In our final receiver function analysis, the time axis is translated into a depth axis using the IASP91 velocity model (Kennett & Engdahl, 1991). This also corrects for moveout, or the difference in arrival time across varying source-station distances (Gurrola et al., 1994).

In light of the high level of microseismic noise in island station data (and seismic data in general), receiver functions are stacked in order to improve the signal-to-noise ratio. Stacks are a summation of moveout-corrected receiver functions at each depth interval. For more on receiver function generation, see Burky et al. (2021) or <https://github.com/alexburky/rflexa>.

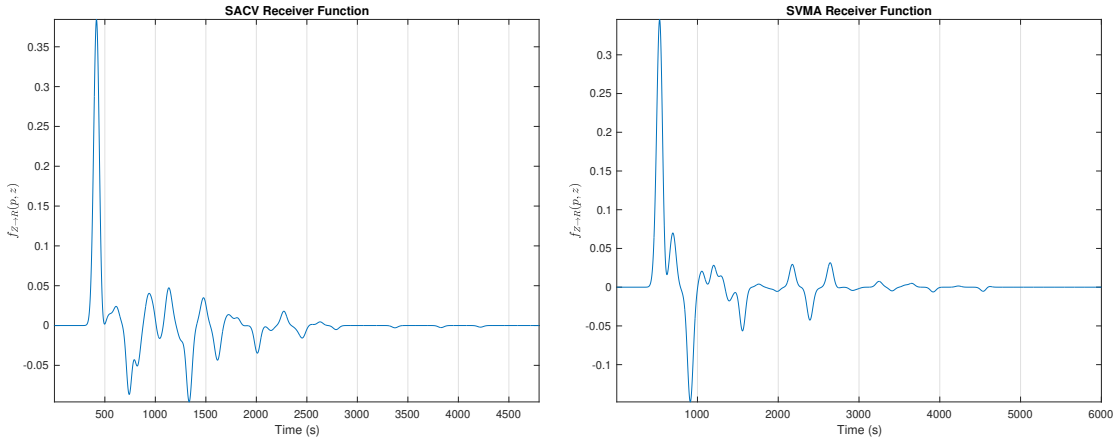


Figure 10: Receiver functions for the 2014 Iquique earthquake at (a) SACV and (b) SVMA.

Results

Results depend on the method of filtration and stacking used. The effect of varying Gaussian widths (GW) on receiver function generation, and thus on stacks, are shown in Fig. 12. Receiver function curves are shifted along the X-axis according to GW value; RFs produced using upper- and lower-limit Gaussian widths with the appropriate $\bar{f}_{Z \rightarrow R}$ values are included for reference in Fig. 11. Positive peaks in $\bar{f}_{Z \rightarrow R}$, the convolutional mapping of vertical to radial component data, represent positive changes in velocity. Lower GW inputs produce larger and smoother peaks, but with lower resolution. At higher GW values, peaks become more distinct but have more background noise. The precision associated with higher GWs are important for constraining the depth at which peaks (and thus velocity discontinuities) appear, but raise questions on the significance of such peaks.

Tracing the influence of Gaussian width values along particular lines of depth reveal that it is difficult to draw conclusions about the specific depth of mantle discontinuities. The depth of the 410 signified by red shading in Fig. 12, for example, decreases with increasing Gaussian width. For the single receiver function, the discontinuity at GW values of 0.3-0.8 disbands altogether beyond values of 1 to become double-peaked.

The frequency-dependence of stack features is further illustrated by looking at the influence of varying the long-period corner frequency of the bandpass filter. New positive velocity spikes appear within the mantle transition zone between frequencies of 0.08 and 0.16 (Fig. 13). Though the strength of the 410 attenuates with decreasing period, the assumed 660 is most prominent at a period just before 6s—a frequency of around 0.15 Hz.

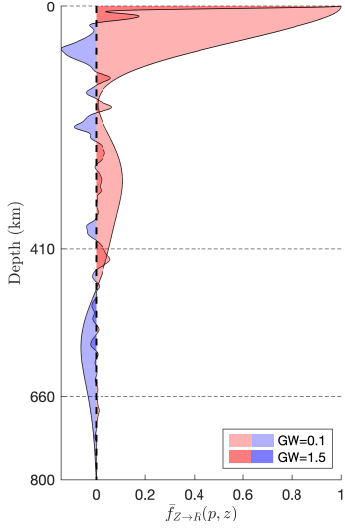


Figure 11: Lower and upper limit Gaussian widths for 2014 Iquique earthquake

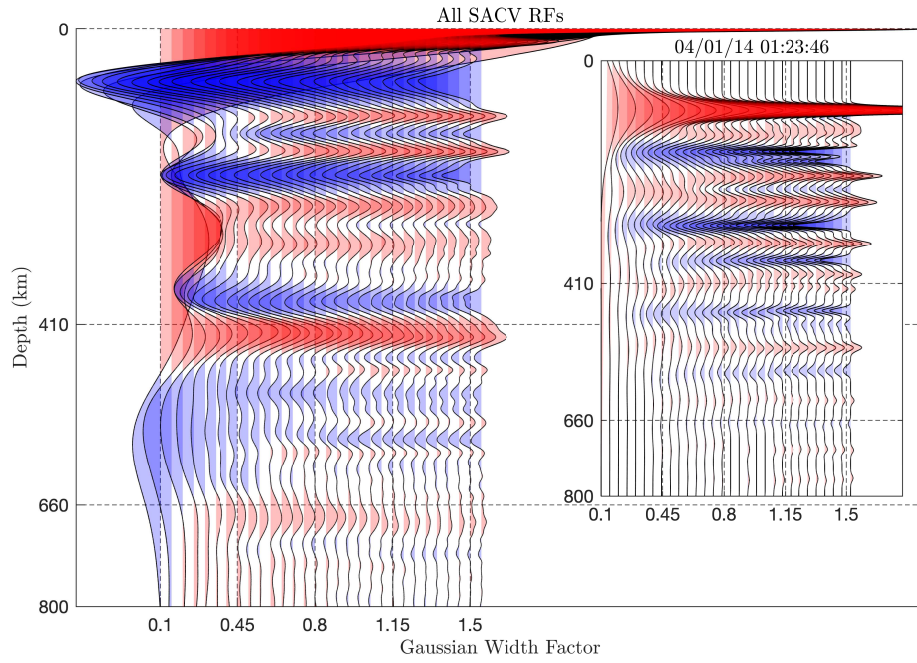


Figure 12: Receiver functions produced by different Gaussian width (GW) factors with fixed corner frequencies of 0.02 Hz to 0.2 Hz. Main axis depicts stacks of RFs computed from all SACV instruments. Overlaid plot shows influence of GW on the RF of a single seismic event (2014 Iquique Earthquake, M_W 7.7, 17 km depth.)

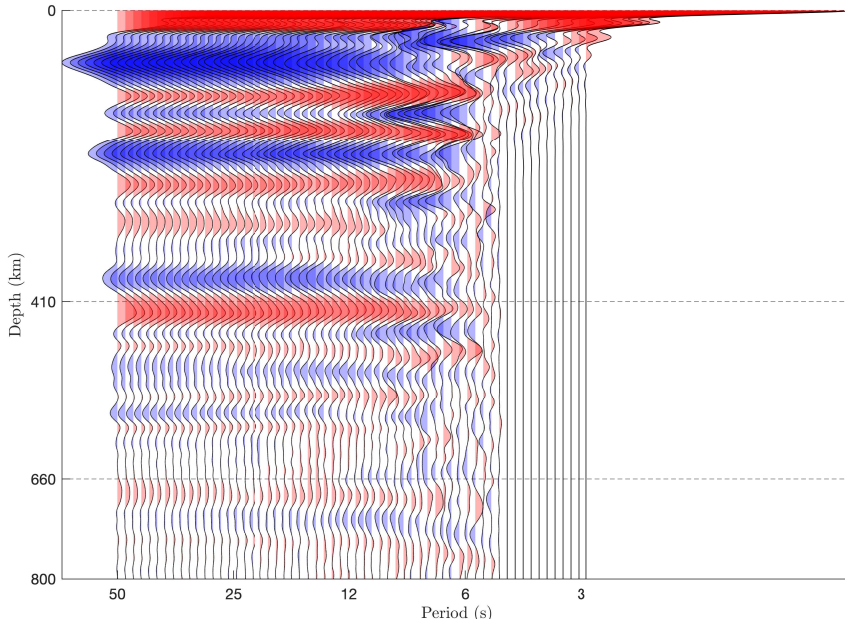


Figure 13: Filter corner frequencies tested on a logarithmic scale from 0.02 Hz to 0.33 Hz and fixed GW of 1.0.

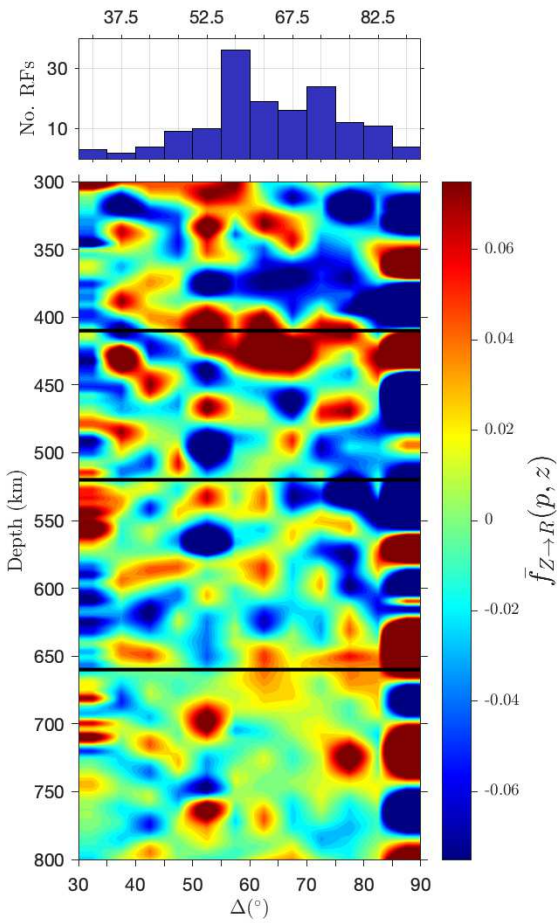


Figure 14: (a) Number of SACV RFs per bin (b) RFs moveout-corrected and binned by source-receiver distance. See aburky/rflexa

as 0.02 Hz to 0.2 Hz. Neither the 410 nor 660 are visible for the first period spanning 05/2000 to 09/2002 (Fig. 15). A weak and depressed 410 appears with the second deployment beginning 09/2002, with a peak centered at 427 km. The 660 is only detectable beginning with deployment IV on 06/2011, where it aligns with the theoretical depth. The 410 is clearest with the most recent deployment beginning on 11/2017, where it lowers by 12 km. This stack incorporates

The 410 is prominent, and depressed, at distances between 50° and 75° (Fig. 14). There is only a weakly visible signal at the 660 with no significant deviation from the expected depth. The strength of discontinuities and number of incorporated receiver functions decreases as stacks move toward the edges of the spatially-retrievable range, reflecting decreasing signal quality. Stacking is also event magnitude-correlated, where higher magnitude events are more likely to meet filtration criteria (Fig. 17).

Station SACV at location code '00' constitutes six separate instrument deployments from May 29, 2000 to the present-day, of which data are available for five. The behaviors of the 410 and 660 vary between stacks made according to these periods. The Gaussian width for all stacks is 1.0, and the filter corner frequencies are set

nearly twice as many receiver functions as those of previous periods ($n = 59$). Still, the 660 only features dubiously, with a peak at 686 km depth.

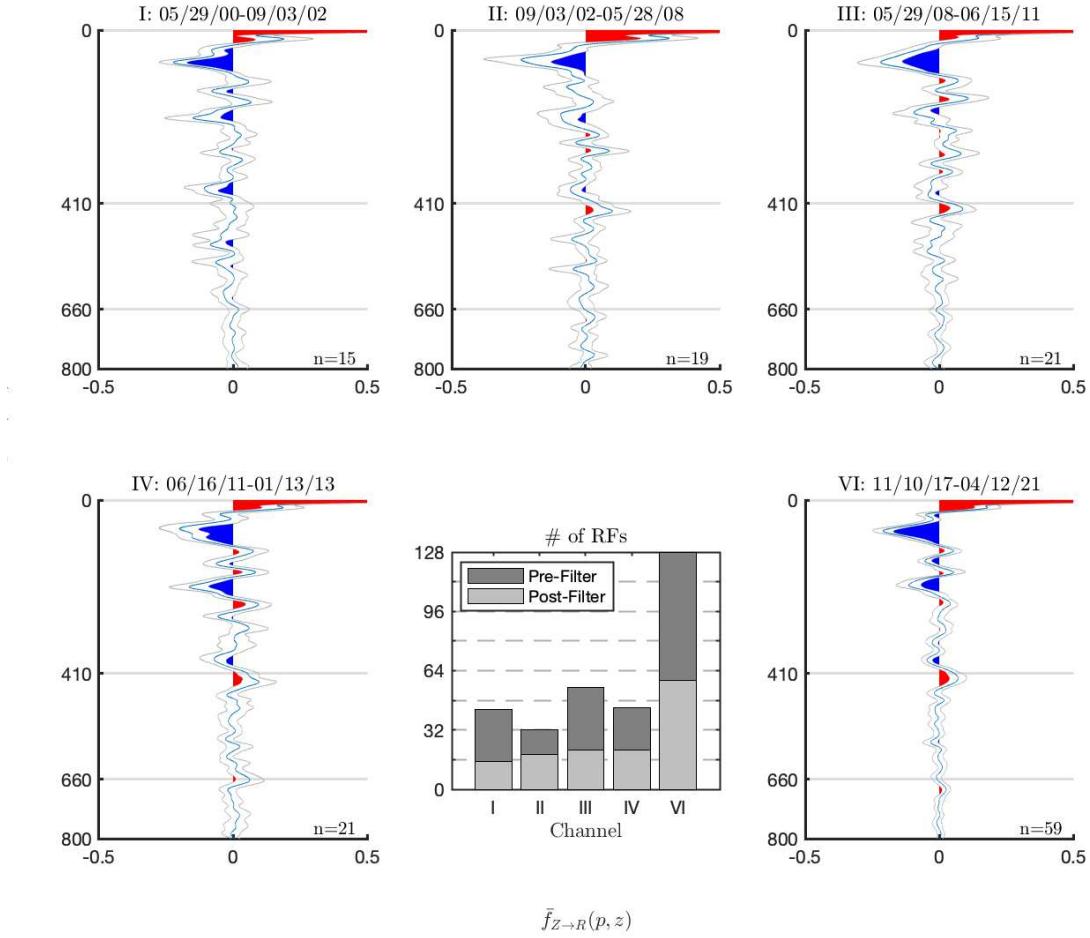


Figure 15: Stacks according to instrument deployment at station SACV Location '00'. There are no data for deployment 5 (from 1-14-2013 to 11-09-2017). Red and blue shading denote positive and negative displacements, respectively. Grey lines trace two standard deviations above and below the mean, obtained through bootstrap re-sampling ($n = 1000$). Number of receiver functions stacked is noted at bottom.

Station SACV employs a second sensor identified by location code '10.' Stacks produced according to the deployment periods of these data reveal positive velocity jumps at the 410 for all groupings. The clearest signal comes from period III, 02/14 to 02/17, where the 410 is 14.7 km deeper than expected, in line with the trend drawn from Location '00' period VI (Fig. 16. Both

incorporate a similar number, large in the context of this dataset, of receiver functions. The 660 does not appear in any Location '10' stacks. The 660 reappears with the sensor at station SVMA where the presence of a peak at exactly 660 km depth is, again, in accordance with the expected discontinuity depth (Fig. 18).

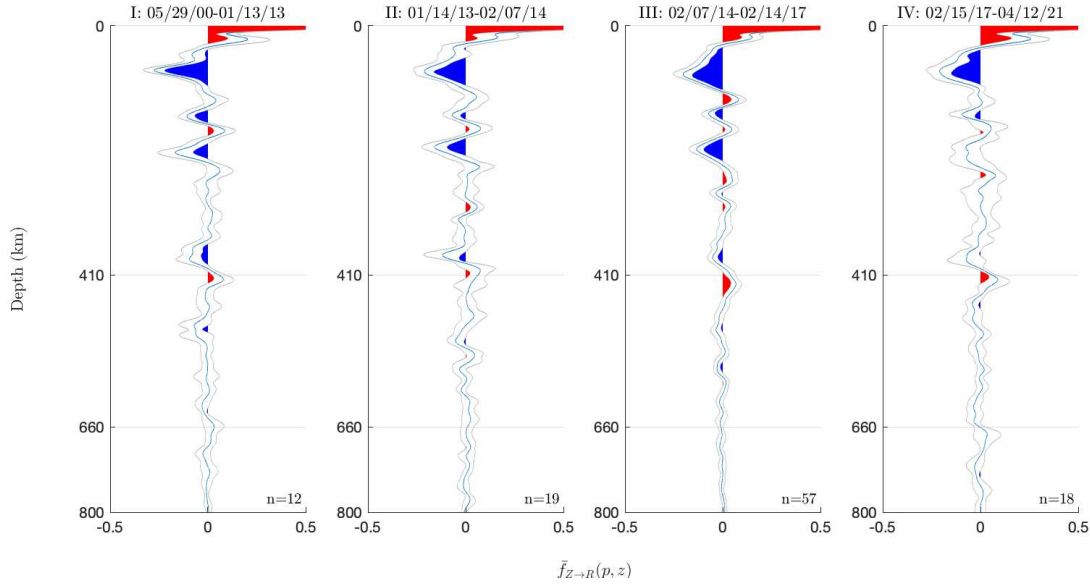


Figure 16: Stacks according to instrument deployment at station SACV Location 10, GW = 1.0, corner frequencies 0.02 Hz—0.2 Hz.

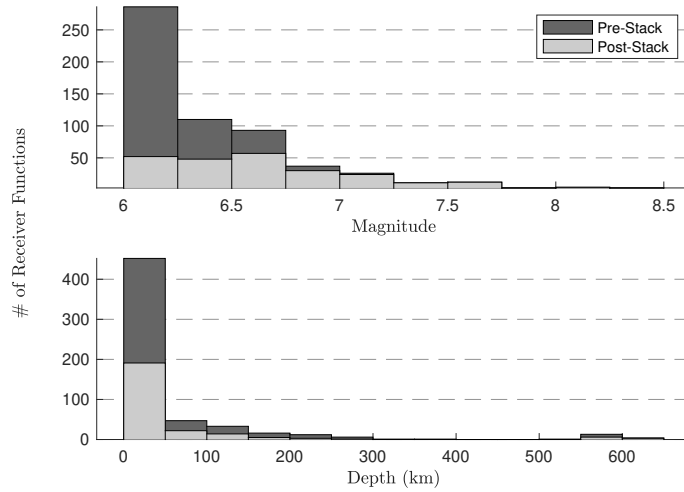


Figure 17: Frequency of (a) magnitudes and (b) depths before and after stack incorporation.

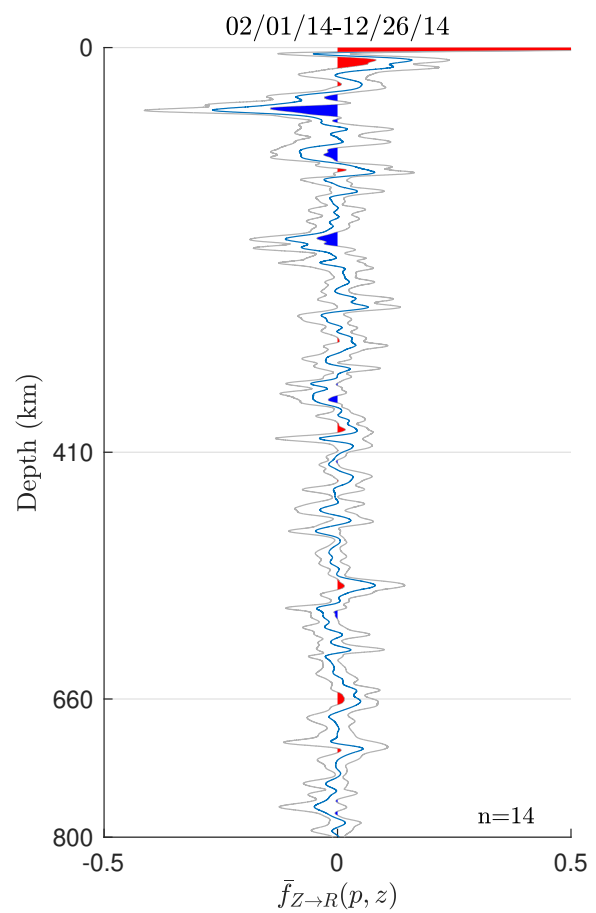


Figure 18: Stack of all SVMA events, GW = 1.0, corner frequency = 0.02 Hz-0.2 Hz

Discussion

The highly variable visibility of the 410 and 660 across stations and time hints at the importance of proper instrumentation when using seismic data to glimpse into Earth's elusive interior. The lack of a clear 660 in all stacks of pre-2011 data may be some combination of instrument implementation flaws and a complex mantle structure at this depth. The influence of instrumentation is apparent in Fig. 10, where receiver functions generated for the same event from different stations yield different results. The frequency dependence of mantle features, seen in the relative strength of the 660 signal at Gaussian widths of around 0.4 to 0.8 (Fig. 12), encourages future work in exploring the response of mantle discontinuities to a variety of filtration methods. The receiver function for the 2014 Iquique Earthquake (Fig. 12 confirms Helffrich & Wood (2001)'s observation that the 410 is reduced at higher frequencies, and that future analyses must resolve this when processing seismic data. In this way, the use of longer-period SS precursors in conjunction with receiver functions may be useful in painting a more-complete image of the mantle.

The finding that the 660 lies at a normal or slightly depressed depth contrasts with previous findings of an uplifted 660 beneath Cape Verde (Vinnik et al. (2012); Saki et al. (2015)). A narrow TZT beneath hotspots is expected if the 660 is dominated by a transition between ringwoodite to perovskite and magnesiowüstite, which has a negative Clapeyron slope, in contrast with the positive Clapeyron slope of the olivine-wadsleyite transition dominating the 410 (Revenaugh & Jordan, 1991). However, the 660 is now understood to be more complicated due to the occurrence of multiple mineral phase transitions. Global surveys of the transition zone beneath hotspots, such as the works of Deuss (2007) and Tauzin et al. (2008), have found evidence of both elevated and lowered 660 discontinuities. A depressed 660 can be explained by the positive Clapeyron slope of the phase transition from majorite to perovskite. Thus, a normal-to-depressed 660 discontinuity doesn't necessarily mean that there is no significant thermal influence underlying the Cape Verde hotspot. Instead, the finding may support that the garnet-perovskite transition is more important than the olivine transition at 660 km depth.

Our observation of a normal transition zone thickness is in agreement with the work of Helffrich et al. (2010). They suggest three explanations: (1) the thermal anomaly overlies the hotspot, (2) there is no thermal anomaly, (3) the thermal conduit is very narrow. They note slower-than-expected arrivals within the transition zone (not necessarily relating to depth). Our observation of a nearly-normal to depressed 660 does not preclude the existence of thermal influence. The finding of an approximately 20 km depression of the 410 suggests that a thermal influence exists and that the weak response of the 660 may be explained by the greater importance of the garnet-perovskite transition (over the olivine transition) in systems with high mantle temperatures (Deuss (2007); Tauzin et al. (2008); Houser et al. (2008)).

Conclusions

Using receiver functions, we find that the seismic velocity discontinuity predicted to occur at 410 km depth is depressed in the transition zone underlying Cape Verde. Less confidently, we also observe a normal-to-depressed 660 km where this signal is strong enough. This contrasts with previous findings of a thin transition zone beneath Cape Verde, which further calls into question the thermal mechanism behind the island's hotspot. Possible explanations include complex and poorly-understood phase transitions occurring at this boundary, resistance of the 660 to thermal influence, or the lack of thermal influence altogether. Future studies should aim to resolve the behavior of the 660 discontinuity below Cape Verde in order to advance our understanding of mantle hotspots and the composition of the inner Earth.

Appendix

All code written to produce the results, analysis, and figures in this thesis are publicly available from my GitHub repository, <https://github.com/amyamatya>, which extends the work of Alex Burky posted on <https://github.com/alexburky/rflexa>.

References

- Allègre, C. J., 2002. Evolution of mantle mixing, *Phil. Trans. R. Soc. London, Ser. A*, **360**(1800), 2411–2431.
- Anderson, D. L., 2000. Thermal state of upper mantle: No rule for mantle plumes, *Geophys. Res. Lett.*, **27**(22), 3623–3626.
- Andrews, J. & Deuss, A., 2008. Detailed nature of the 660 region of the mantle from global receiver function data, *J. Geophys. Res.*, **113**(B6), 1–12.
- Bina, C. R. & Helffrich, G., 1994. Phase transition clapeyron slopes and transition zone seismic discontinuity topography, *J. Geophys. Res.*, **99**, 15853–15860.
- Burke, K. & Wilson, J. T., 1972. Is the African plate stationary?, *Nature*, **239**, 387–390.
- Burky, A., Irving, J. C. E., & Simons, F. J., 2021. Mantle transition zone receiver functions for Bermuda: Automation, quality control, and interpretation, *J. Geophys. Res.*, **126**, e2020JB020177, doi: 10.1029/2020JB020177.
- Crotwell, H. P. & Owens, T. J., 2005. Automated receiver function processing, *Seismol. Res. Lett.*, **76**(6), 702.
- Davies, G. F., 1999. *Dynamic Earth: Plates, Plumes, and Mantle Convection*, Cambridge Univ. Press, Cambridge, UK.
- Deuss, A., 2007. Seismic observations of transition-zone discontinuities beneath hotspot locations, *Plates, Plumes and Planetary Processes*, **430**, 121–135.
- Flanagan, M. P. & Shearer, P. M., 1998. Global mapping of topography on transition zone velocity discontinuities by stacking ss precursors, *J. Geophys. Res.*, **103**, 2673–2692.
- Gao, S. S. & Liu, K. H., 2014. Mantle transition zone discontinuities beneath the contiguous united states, *J. Geophys. Res.*, **119**, 6452–6468.

- Gu, Y. J. & Dziewonski, A. M., 2002. Global variability of transition zone thickness, *J. Geophys. Res.*, **107**, ESE 2–1–ESE 2–17.
- Gurrola, H., Minster, J. B., & Owens, T., 1994. The use of velocity spectrum for stacking receiver functions and imaging upper mantle discontinuities, *Geophys. J. Int.*, **117**, 427–440.
- Helffrich, G., Faria, B., Fonseca, J. F. B. D., Lodge, A., & Kaneshima, S., 2010. Transition zone structure under a stationary hot spot: Cape Verde, *Earth Planet. Sci. Lett.*, **289**(1–2), 156–161.
- Helffrich, G. R. & Wood, B. J., 2001. The Earth's mantle, *Nature*, **412**(6486), 501–507.
- Holm, P. M., Grandvoinet, T., Friis, J., Wilson, J. R., Barker, A. K., & Plesner, S., 2008. An 40Ar–39Ar study of the Cape Verde hot spot: Temporal evolution in a semistationary plate environment, *J. Geophys. Res.*, **113**, 1–22.
- Houser, C., Masters, G., Flanagan, M., & Shearer, P., 2008. Determination and analysis of long-wavelength transition zone structure using ss precursors, *Geophys. J. Int.*, **174**, 178–194.
- Ito, E. & Takahashi, E., 1989. Postspinel transformations in the system $mg_2sio_4-fe_2sio_4$ and some geological implications, *J. Geophys. Res.*, **94**, 10637–10646.
- Kennett, B. L. N. & Engdahl, E. R., 1991. traveltimes for global earthquake location and phase identification, *Geophys. J. Int.*, **105**, 429–465.
- Kind, R., Yuan, X., & Kumar, P., 2012. Seismic receiver functions and the lithosphere–asthenosphere boundary, *Tectonophysics*, **536–537**, 25–43.
- Lawrence, J. F. & Shearer, P. M., 2006. A global study of transition zone thickness using receiver functions, *J. Geophys. Res.*, **111**, 1–10.
- Ligorria, J. P. & Ammon, C. J., 1999. Iterative deconvolution and receiver function estimation, *B. Seismol. Soc. Am.*, **89**(5), 1395–1400.
- Liu, X. & Zhao, D., 2014. Seismic evidence for a mantle plume beneath the Cape Verde hotspot, *Intern. Geol. Rev.*, **54**(10), 1213–1225.
- Montelli, R., Nolet, G., Dahlen, F. A., & Masters, G., 2006. A catalogue of deep mantle plumes: New results from finite-frequency tomography, *Geochemistry, Geophysics, Geosystems*, **7**, 1–69.
- Morgan, W. J., 1971. Convection plumes in the lower mantle, *Nature*, **306**, 42–43.
- Revenaugh, J. & Jordan, T. H., 1991. Mantle layering from scs reverberations. 3. The upper mantle, *J. Geophys. Res.*, **96**(B12), 19781–19810.
- Saki, M., Thomas, C., Stuart, E. J., & Lessing, S., 2015. Topography of upper mantle seismic discontinuities beneath the North Atlantic: The Azores, Canary, and Cape Verde plumes, *Earth Planet. Sci. Lett.*,

409.

- Shearer, P., 2009. *Introduction to Seismology*, Cambridge Univ. Press, Cambridge, UK.
- Shearer, P. M., Flanagan, M. P., & Hedlin, M. A. H., 1999. Experiments in migration processing of ss precursor data to image upper mantle discontinuity structure, *J. Geophys. Res.*, **104**, 7229–7242.
- Silveira, G., Vinnik, L., Stutzmann, E., Farrad, V., Kiselev, S., & Morais, I., 2010. Stratification of the earth beneath the azores from p and s receiver functions, *Earth Planet. Sci. Lett.*, **299**, 91–103.
- Tauzin, B., Debayle, E., & Wittlinger, G., 2008. The mantle transition zone as seen by global pds phases: No clear evidence for a thin transition zone beneath hotspots, *J. Geophys. Res.*, **113**, 1–17.
- Vinnik, L., Silveira, G., Kiselev, S., Farra, V., Weber, M., & Stutzmann, E., 2012. Cape Verde hotspot from the upper crust to the top of the lower mantle, *Earth Planet. Sci. Lett.*, **319-320**, 259–268.
- Zhao, D., 2001. Seismic structure and origin of hotspots and mantle plumes, *Earth Planet. Sci. Lett.*, **192**, 251–265.